Construction of the Tortuosity Factor from Porosimetry

S. C. CARNIGLIA[1]

*Center for Technology, Kaiser Aluminum & Chemical Corporation, 6177 Sunol Blvd.,
Pleasanton, California 94566*

The tortuosity factor for volume diffusion in porous solids, τ, is constructed mathematically from properties of their connected porosity based on Hg porosimetry and related measurements. Noncylindrical diffusion paths are identified and incorporated in the construction. The resulting equation, $\tau = x \cdot (0.92y)^{1+\varepsilon}$, for the first time makes possible the computation of τ without recourse to diffusion measurement. The term x is a function of pore volume; y is derived from porosimetry and surface area data; and ε is obtained from ordinary $D(\rho)$ vs ρ data where ρ is pore radius. The computed τ agrees with diffusion-determined values for many catalysts and other oxidic materials. © 1986 Academic Press, Inc.

I. INTRODUCTION

The tortuosity factor τ in porous solids connects the "effective" or observed diffusivity to a reference diffusivity, commonly by $D_{\text{eff}} = D(\mathring{\rho}) \cdot f/\tau$. Here f is the total connected-pore volume fraction and $\mathring{\rho}$ is a mean radius of the pores of the material. Often $D(\mathring{\rho})$ can be written $D_b G(\mathring{\rho})$ or $D_b L(\mathring{\rho})$, where D_b is the bulk diffusivity of the operating diffusant system and G and L are continuous functions of pore radius for gaseous *(1, 2)* and for liquid *(3–5)* diffusant systems.

The determination of τ by experimental measurement of D_{eff} and use of the above equation seems clouded by historical choice of $\mathring{\rho}$ or of $D(\mathring{\rho})$. Nonetheless, τ clearly varies over a wide range from material to material *(6)*. Its earliest conception as a simple matter of diffusion path tortuosity *(7)* was soon found insufficient; yet other theoretical approaches (e.g., *(8, 9)*) produced relatively constrained values from idealized pore models and could nowise relate the wide range found to instrumentally measurable properties of porosity *(6)*. The unique approach taken by Wakao

and Smith *(10)* resulted in a deduction that $\tau = 1/f$, variable to be sure but not sustained as a general form by the large body of empirical data *(6)*. As recently as 1985 *(11)*, the only recourse for the determination of τ was still by diffusion measurements. Those techniques are so difficult that many workers in catalysis submit to alternatives which impede their best kinetic analytical efforts.

There should be a way of computing τ from measurable porosity characteristics. This concept was included in rudimentary form in an earlier paper treating catalyst reactivity *(12)*; but that form soon evidenced a need for refinement *(13)*. Notice has also been taken of the common practice *(11, 14, 15)* of modeling diffusion paths through porous bodies as always cylindrical, i.e., of constant radius throughout. That idealized model has to be superseded. Finally, the correct selection of a reference diffusivity, e.g., $D(\mathring{\rho})$, becomes of no small importance itself.

The purpose of this paper is accordingly to present a mathematical construction of τ founded on measurable material properties; and in so doing to utilize a realistic description of porosity and a sound interpretation of the yield of common measurement tools. Uniform, isotropic materials will be assumed. Fick's 1st Law will be used to de-

[1] Present mailing address: 115 Wilshire Court, Danville, Calif. 94526.

scribe volume diffusion, but this should not be misleading. Diffusion controlled by surface migration is not addressed. Nor is zeolite-type intracrystalline microporosity; otherwise, the results should apply to most type of porous materials.

II. RELATIONS AMONG PROPERTIES OF POROSITY

It is necessary first to catalog the properties of connected porosity on which τ will depend. Some of these are ordinarily measured in material characterization. Some will be inferred but fall into a mathematical framework such that they can be profitably utilized even though unmeasured.

1. Properties of Total Connected Porosity

"Connected porosity" is depicted as a random network of interconnected cavities of unspecified sizes and shapes, called "pores." Every pore is seen as bounded by two branching intersections or "junctions" of high connectivity, i.e., each with a multiplicity of other pores. Let the sum of all pores in a given body be $\bar{n}^3$ per cm^3 of nominal body volume. Then $\bar{n}^2$ pores intersect 1 cm^2 of body surface and $\bar{n}$ connected pores can be identified with 1 cm of body length, in any direction.

Every pore can be characterized in concept by its length l_p between the center points of its two bounding junctions. A diffusion flux through each pore would be predominantly parallel to this l_p, i.e., from junction to junction. Though each l_p is oriented uniquely, random orientations are assumed overall. Let l be the scalar average of all l_p.

Each pore also has a volume, v_p, from which a mean cross section area for diffusion through the pore can be derived. If $\bar{v}$ is the average of all v_p, then the total void volume fraction is $f = V_s d = \bar{n}^3 \bar{v}$. Here f is in cm^3/cm^3; V_s is the total specific volume in cm^3/g of body, and d is the nominal body density in g/cm^3. These latter quantities are directly measurable, V_s, for example, by mercury porosimetry and d, for example,

by measuring body weight and dimensions or by weighing in nonpenetrating immersion liquids.

If $\bar{s}$ is the average of the wall areas s_p of all pores in a given body, then the total specific surface area, S_s in cm^2/g, is accounted for by $S_s d = \bar{n}^3 \bar{s}$. This S_s is directly measurable, for example, by simple BET nitrogen adsorption.

Mensuration formulae adopted for pore volume and surface area are of nominal "cylindrical" form (6, 7, 11, 14, 15), but are applied to overall mean dimensions as $\bar{v} = \pi \bar{\rho}^2 l$ and $\bar{s} = 2\pi \bar{\rho} l$ without imputing cylindricity to every pore. In these terms V_s and S_s are evident, and their ratio is $S_s/V_s = 2/\bar{\rho}$. Early measurements of V_s and S_s seemed to support this relation (6), but uncertainty was introduced by the approximations then used for the overall mean pore radius $\bar{\rho}$. The recent compilation and further contributions of Davis (16) may seem at least as much to undermine as to support this simple ratio. But the determination of $\bar{\rho}$ in Section IV will remove apparent experimental discrepancies.

The underlying mensuration formulae, however, omit an important correction. Pores have finite cross sections, hence when they intersect both volume and surface area are lost relative to what these would be if each pore were separately terminated by cuts perpendicular to the extremities of its l_p (7). Simple pore-junction models were sketched and the average volume loss estimated for all (random) angles among the several pores joined, arriving at about $5\pi\bar{\rho}^3/4$ per pore of average radius $\bar{\rho}$. It can be anticipated that this loss will affect the tortuosity factor. By trial in an equation to be presented later, it was found that meeting the boundary condition $\tau = 1.0$ when $f = 1.0$ requires restating this loss as about $4\pi\bar{\rho}^3/3$ or as $\pi\bar{\rho}^2 l \cdot 4\bar{\rho}/3l$ per pore on average. This is only 6% greater than the former estimate. Its adoption is necessitated by the stated boundary condition, not by the models from which it was approached.

The total volume correction for pore junctions then becomes $\bar{n}^3\pi\bar{\rho}^2\bar{l} \cdot 4\bar{\rho}/3\bar{l}$, and the corrected total pore volume fraction is then $f = V_s d = \bar{n}^3\pi\bar{\rho}^2\bar{l}(1 - 4\bar{\rho}/3\bar{l})$. The corresponding surface area loss will not be needed for calculating τ. It is simply assumed to be such as not to disturb the ratio $S_s/V_s = 2/\bar{\rho}$ when the corrected $V_s d$ and $S_s d$ are both employed. This assumption too will be validated by the determination of $\bar{\rho}$ in Section IV.

2. Pore Chains as Independent Diffusion Paths

The equation for f given last above includes the terms $\bar{n}^3$, $\bar{\rho}$, and $\bar{l}$; but none of these is directly measurable. The following will add to the foundations underlying τ, while permitting the elimination of some of these immeasurables.

Consider a right cylindrical porous body of length Z cm in the direction of uniaxial diffusion and of area 1 cm² on each of its faces. Assume that all its pores participate in diffusion; hence there are $\bar{n}^2$ diffusion paths in this body, each of $\bar{n}$ pores per cm connected in one continuous chain substantially parallel to the Z axis (6, 14, 15). This is a formal assumption. Furthermore, in ignoring blind or inaccessible pores, the assumption has in some cases been contraindicated (17–19), and some models have been designed to account for pores contributing to total volume but not to diffusion (20, 21). Nevertheless, this assumption provides a limiting model for the maximum possible mass transport through a given porosity.

Useful corollaries ensue. The mean projection of randomly oriented pores on the diffusion axis is $2\bar{l}/\pi$ per pore; this is the mean of $\bar{l}\cos\alpha$ for $0 \le \alpha \le \pi/2$, where α is the acute angle made between the direction of each l_p and that axis. The cumulative length of a macroscopically "straight" chain of $\bar{n}$ connected pores (viz., a shortest diffusion path) is $\overline{n\bar{l}}$, while its projected body length is accordingly $2\overline{n\bar{l}}/\pi = 1$ cm; hence the shortest path through Z cm of

body is $\pi Z/2$ cm long. It also follows that $\bar{n} = \pi/2\bar{l}$. Given the immense number of opportunities for path selection implied by $\bar{n}^3$ and that the path length condition $\pi Z/2$ can be met even by a semicircular path of diameter of curvature Z, it is also assumed that all real diffusion paths are sensibly equal in length to this shortest path (6, 7). The power of these relationships in eliminating variables will be exercised presently.

3. Subdivision of Porosity into Groups: Group Properties

Pores have so far been considered as comprised of an unspecified range of individual effective radii, ρ_p. To approach pore radius as potentially measurable, collect or group together all pores in a given body whose effective radii fall within a very narrow interval about a selected ρ_i such that ρ_i can represent the mean of this interval. If there are n_i^3 pores in the interval per cubic centimeter of body, of individual volumes averaging $\bar{v}_i$ and surface areas averaging $\bar{s}_i$, then the "group" volume fraction is $\Delta f_i = \Delta V_i d = n_i^3\bar{v}_i$ and the "group" surface area is $\Delta S_i d = n_i^3\bar{s}_i$. The total porosity can then be described as the sum of m contiguous pore groups of progressively increasing ρ_i, viz., indexed by $i = 1$ to $i = m$. Here ρ_1 represents the smallest group present which contributes a detectibly nonzero ΔV_1 or ΔS_1; and ρ_m represents the maximum size group present, likewise contributing a detectibly nonzero ΔV_m or ΔS_m. The group properties described above are obviously additive.

It is taken as *Axiom 1* that some group mean pore length l_i exists such that the volume and surface mensuration formulae of Subsection 1 also apply to each group severally. But the pore intersections dictating l_i in a common network of $\bar{n}^3$ pores/cm³ will be in general far more frequent than if the total porosity consisted of only a single group of n_i^3 pores/cm³. This means that the corrected pore volume must be written for any ith group as $\Delta f_i = \Delta V_i d = n_i^3\pi\rho_i^2 l_i(1 - 4\bar{\rho}/3\bar{l})$, wherein the bracketed quantity is a mean property of the common total net-

work. Quite evidently, when this Δf_i is summed over all i to give f, the result agrees with that approached from descriptors of the total porosity. The same qualities are imputed to the construction and summation of a corrected group surface area $\Delta S_i d$; and it follows from this axiom that $\Delta S_i / \Delta V_i = 2/\rho_i$. Thus group properties are taken axiomatically to comprise sets that are mathematically consistent with the properties of total porosity, and which yield those by summing.

Axiom 2 concerning pore groups relates to their analysis, severally, into independently acting, interpenetrating sets of diffusion paths. This axiom postulates that every relationship of Subsection 2 can be rewritten separately for every one of the m pore groups comprising a total porosity. Thus every ith group can be treated for uniaxial diffusion as if it provides n_i^2 diffusion paths/cm^2, each consisting of n_i connected pores per centimeter in the diffusion direction Z. Each path length in Z cm of body remains $\pi Z/2$ cm, and $n_i = \pi/2l_i$ as previously. The signal difference between these group relationships and those of Subsection 2 is that here every ith-group diffusion path consists entirely of pores of radius close to ρ_i.

This axiom is operational, not pictorially descriptive. It is implicit in all prior "cylindrical-path" diffusion models (*6, 7, 11, 14, 15*). Further, it can be shown to lead mathematically to the same mass transport rate through a given porosity as that obtained when overall pore properties are used (Section III). It is here adopted on these grounds.

4. Consolidation of Geometrical Relations

Overall volume fraction. The corrected equation for f of Subsection 1 can be combined with $\bar{n} = \pi/2\bar{l}$ to eliminate $\bar{n}^3$, yielding:

$$f = V_s d = (\pi^4/8)(\bar{\rho}/\bar{l})^2 \cdot (1 - 4\bar{\rho}/3\bar{l}). \quad (1)$$

This equation relates the parameter $(\bar{\rho}/\bar{l})$ solely to the total volume fraction; it has

only one physically acceptable root. Fig. 1 includes a plot of the inverse, viz., of the ratio $(\bar{l}/\bar{\rho})$, and a curve of $(1 - 4\bar{\rho}/3\bar{l})$ computed from Eq. (1), vs $f = V_s d$ on a log scale. Thus the immeasurables $\bar{n}$ and $\bar{l}$ have been replaced by a mean pore aspect ratio which is determined by V_s and d alone. This computed ratio is independent of $\bar{\rho}$ per se, thus applies to any pore size distribution.

Group volume fraction. The corresponding deduced equation for Δf_i of Subsection 3 is likewise combined with $n_i = \pi/2l_i$ to yield

$$\Delta f_i = \Delta V_i d = (\pi^4/8)(\rho_i/l_i)^2 \cdot (1 - 4\bar{\rho}/3\bar{l}). \quad (2)$$

For a given material, if V_s and d are measured the last bracket above is determined by Eq. (1) or Fig. 1. Then Eq. (2) relates the group pore aspect ratio (ρ_i/l_i) uniquely to the group volume fraction. The correct measurement of ΔV_i by Hg porosimetry is necessarily deferred (Section IV), but that measurement is confidently expected. The solution of Eq. (2) is independent of both ρ_i and $\bar{\rho}$ per se.

Surface/volume ratio. This ratio will become important in Section IV. In rearranged form, corrected surface area/volume ratios are recapitulated as

$$S_s = 2V_s/\bar{\rho} \quad \text{and} \quad \Delta S_i = 2\Delta V_i/\rho_i. \quad (3a)$$

Invoking $S_s = \sum_1^m \Delta S_i$ and $V_s = \sum_1^m \Delta V_i$, it is readily derived that

$$\frac{1}{\bar{\rho}} = \frac{\sum\limits_1^m \Delta V_i/\rho_i}{V_s} \equiv (\overline{1/\rho_i}), \quad (3b)$$

wherein the identity sign means $(\overline{1/\rho_i})$ is defined by its preceding ratio.

Diffusion path relations. Recapitulating from Subsection 2, a total porosity comprised of $\bar{n}^3$ pores/cm^3 provides $\bar{n}^2$ uniaxial diffusion paths/cm^2, each of "tortuous" length $\pi Z/2$ cm over a nominal body length of Z cm. But each path is of a mean radius $\bar{\rho}$ cm which might be the mean of widespread
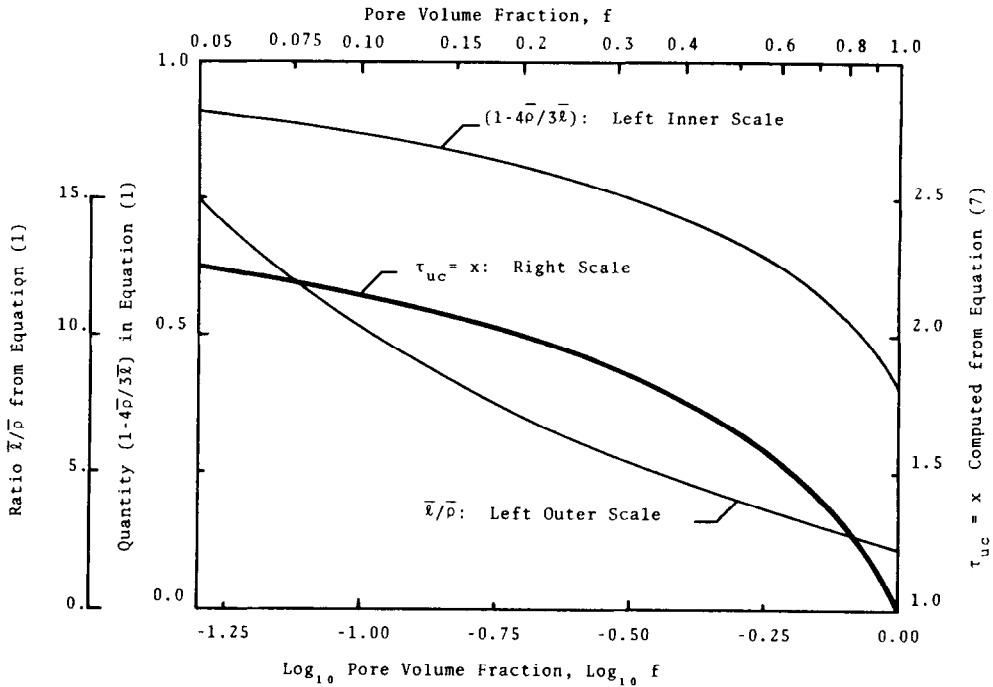
FIG. 1. Mean pore parameters and derived τ_{uc} vs log pore volume fraction.

ρ_p values unless *Axiom 2* is obeyed by nature. A mass transport through this total porosity can be computed using these relations together with a mean path cross section area of $\pi\bar{\rho}^2$.

Of still greater utility but explicitly subject to *Axiom 2*, a pore-size group comprised of n_i^3 pores/cm³ provides (from Subsection 3) n_i^2 uniaxial diffusion paths/cm², each of tortuous length $\pi Z/2$ cm over a nominal body length of Z cm, while every path is of relatively homogeneous radius about ρ_i cm. From this base the mass transport through the total porosity can be obtained by summing that computed for each *i*th group over all m values of i, with path cross section areas $\pi\rho_i^2$.

The above two anticipated approaches to computing diffusional mass transport should yield the same result. This presumption will be tested once in Section III; then either approach will be validated for subsequent use as may be convenient.

III. CONSTRUCTION OF τ_c FOR CYLINDRICAL DIFFUSION PATHS

The construction of τ_c per se depends solely on the preceding measurables. It is therefore presented here in sequence, before preparing for τ in general.

A working definition of a "cylindrical" diffusion path is that the variation in its radius does not exceed the width of a pore group radius interval, hence each group path radius can be treated as of constant ρ_i as a reasonable approximation. *Axiom 2* of Subsection II.3 may resemble a presumption of path cylindricity, but in fact this is not necessarily so. Criteria for path cylindricity or noncylindricity will be clearly developed out of Hg porosimetry data in Section IV. Until then, path cylindricity will here be temporarily imposed as a condition of the simplest construction of a tortuosity factor which is accordingly called τ_c. Real porous materials satisfying this condition are not especially common, but they do ex-

ist. Intuitively, they are most likely to be materials exhibiting unimodal porosity.

1. Unimodal Porosity with Cylindrical Paths: τ_{uc}

Set up steady-state uniaxial diffusion through a cylindrical porous specimen, such that a diffusant concentration difference Δc (moles/cm^3) exists over nominal specimen length Z cm. The mean concentration gradient through each diffusion path is then $2\Delta c/\pi Z$. Using Fick's 1st Law to describe volume diffusion through a single group path of mean radius ρ_i, the mass transport rate $N_{\Pi i}$ in that one path is

$$N_{\Pi i} = -\pi\rho_i^2 D(\rho_i) \cdot 2\Delta c/\pi Z. \qquad (4)$$

Here $D(\rho_i)$ is as suggested by Section I in cm^2/sec. There are n_i^2 such group paths/cm^2 of normal specimen face. Multiply by this and replace n_i^2 by $(\pi/2l_i)^2$ to obtain the areal mass transport rate through the entire ith pore group, N_{Ai}, in moles/sec per cm^2 of specimen face:

$$N_{Ai} = -(\pi^2\rho_i^2/2l_i^2) \cdot D(\rho_i) \cdot \Delta c/Z. \quad (5a)$$

But $(\pi^2\rho_i^2/2l_i^2)$ is, from Eq. (2), $4\Delta f_i/\pi^2(1 - 4\bar{\rho}/3\bar{l})$. Insert this in the above, replace $4/\pi^2$ by $1/2.4674$, and rearrange to yield

$$N_{Ai} = -\frac{\Delta c/Z}{2.4674(1 - 4\bar{\rho}/3\bar{l})} \cdot \Delta f_i D(\rho_i).$$

$$(5b)$$

Now sum Eq. (5b) over all i to obtain the areal mass transport rate N_A through the total porosity. Only the last product $\Delta f_i D(\rho_i)$ is affected, becoming $\sum_1^m \Delta f_i D(\rho_i)$.

This is the same as $f \cdot \left[\sum_1^m \Delta f_i D(\rho_i) \middle/ \sum_1^m \Delta f_i\right]$

or $V_s d \cdot \left[\sum_1^m \Delta V_i D(\rho_i) \middle/ \sum_1^m \Delta V_i\right]$. Either bracketed ratio of summations defines a mean D, called here $\overset{\circ}{D}$; and this $\overset{\circ}{D}$ is fundamental to correct usage of the tortuosity factor in any diffusion equation.

In the unique case of unimodal porosity,

however, if the modal pore-size interval is sufficiently narrow that $D(\rho_i)$ is linear with ρ_i over all i, then $\sum_1^m \Delta f_i D(\rho_i)$ can be expressed instead as $f \cdot D\left(\sum_1^m \Delta f_i \rho_i \middle/ \sum_1^m \Delta f_i\right)$ $= f \cdot D(\overset{\circ}{\rho})$. This substitution is permissible only for unimodal porosity, and even then may be only approximate.

With $D(\overset{\circ}{\rho})$ so determined in this case, then the summation of Eq. (5b) becomes

$$N_A = -\frac{f}{2.4674(1 - 4\bar{\rho}/3\bar{l})} \cdot D(\overset{\circ}{\rho}) \cdot (\Delta c/Z);$$

$$(6)$$

from which by the conventional notation of Section I,

$$\tau_{uc} = 2.4674(1 - 4\bar{\rho}/3\bar{l}). \qquad (7)$$

Recall that $(1 - 4\bar{\rho}/3\bar{l})$ is a function of f alone by Eq. (1), as graphed in Fig. 1. Hence τ_{uc} is also a function uniquely of $f = V_s d$. Figure 1 also includes the curve of τ_{uc} computed from Eqs. (7) and (1). This curve goes to 1.0 at $f = 1.0$ as it must (viz., the boundary condition referred to earlier), and it rises to above 2 at low f.

2. Construction of τ_c for Any PSD with Cylindrical Paths

In the above derivation of τ_{uc}, the sole consequence of specification of unimodal porosity was the permissibility of replacing $\overset{\circ}{D}$ as defined there by $D(\overset{\circ}{\rho})$ as an approximation. When the pore size distribution (PSD) is bi- or multimodal or otherwise broad, that substitution is patently unjustified: $\overset{\circ}{D}$ must appear in Eq. (6). But otherwise, Eqs. (4)–(7) are quite unaffected; hence $\tau_c \equiv \tau_{uc}$.

The term $(1 - 4\bar{\rho}/3\bar{l})$ appearing in Eq. (7) is a computational nuisance, however, and can be simplified. The curve of τ_{uc} of Fig. 1 was replotted vs f on a linear scale, with the resulting discovery of near-linear behavior over the entire range $0.05 \leq f \leq 0.95$. This range brackets all solid catalysts of practical interest. A linear curve approximating

Eq. (7) within ±2% over this range is expressed simply as, for any PSD with cylindrical diffusion paths:

$$\tau_c = 2.23 - 1.13V_s d = x$$
$$(0.05 \leq V_s d \leq 0.95). \quad (8)$$

Thus *if* cylindrical diffusion paths prevail in a given material, the only physical measurements necessary to determine its tortuosity factor are V_s and d. Much larger tortuosity factors than 2.2 are on record, however, implying that many real materials exhibit noncylindrical paths (*6*). Anticipating the usefulness of Eq. (8) in deriving τ for that case (Section V), the designation "*x*" has also been assigned, above, to this function. The following will complete the treatment of τ_c and $\overset{\circ}{D}$.

3. Identity of Two Approaches to τ_c

In Subsection II.4 an alternative approach to Eqs. (4)–(8) was suggested, based on the properties of a total porosity instead of on its subdivision first into *m* contiguous pore-size groups. It will be important later to have shown that the two approaches yield the same tortuosity factor.

Only the approach given above includes a fundamental derivation of $\overset{\circ}{D}$, however. It should be apparent that the general use of τ *must* be stated as $D_{eff} = \overset{\circ}{D} \cdot f/\tau$, and that the relation $D_{eff} = D(\overset{\circ}{\rho}) \cdot f/\tau$ given in Section I is permissible *only* for unimodal porosity. That distinction has escaped notice in most prior determinations of τ by diffusion measurements (*6*), an oversight responsible for major errors in the computed τ for materials of broad PSD (*12, 13*). In the present exercise, as well as later, $\overset{\circ}{D}$ as defined in Subsection 1 above must be incorporated.

With that provision, to derive τ_c from the properties of total porosity one first replaces ρ_i^2 by $\bar{\rho}^2$ in Eq. (4). In the next operation one goes directly to N_A by use of the multiplier $\bar{n}^2$ and $\bar{n}^2 = (\pi/2\bar{l})^2$, then notes from Eq. (1) that $(\pi^2\bar{\rho}^2/2\bar{l}^2) = 4f/\pi^2(1 - 4\bar{\rho}/3\bar{l})$. The result is that Eq. (6) is repeated exactly (but incorporating $\overset{\circ}{D}$); and it follows

that τ_c is again given by Eq. (7) or (8). Thus both approaches give the same tortuosity factor.

This observation permits use of this alternative approach in Section V, a matter of no little convenience. It also implies a validation of *Axiom 2* given previously, in that Eqs. (4)–(8) depended explicitly on this axiom while the alternative approach to τ_c did not assume it.

IV. Hg POROSIMETRY[2]; NONCYLINDRICAL DIFFUSION PATHS

Measurement of several parameters of the preceding Sections has been deferred, to be treated here. Mercury intrusion porosimetry can determine a reasonably accurate ρ_i and ΔV_i for each pore size group in a given specimen, and can sum ΔV_i over *i* values at will (*6, 10–12, 16, 20*). It can also be used to determine $\bar{\rho}$ and $\overset{\circ}{\rho}$ and to assist in obtaining $\overset{\circ}{D}$. For all of these, however, the output of the instrument as well as of BET measurement of S_s has to be consistently interpreted. The further signal contribution of Hg porosimetry here will be the disclosure of noncylindrical diffusion paths in porous materials and assistance in the final construction of τ to follow.

1. Instrument Use and Interpretation

Mercury bathing an evacuated specimen has access in principle to its entire interconnected porosity via every pore intersecting its external surface. But for most nonmetallic materials the interfacial contact angle is such as to resist Hg penetration of the pores. On application of increasing pressure P on the mercury, intrusion successively fills intricate "channels" or pore networks of progressively decreasing minimum cross sections, i.e., in the nomi-

---

[2] For introduction to the theory and practice of Hg porosimetry, also of BET surface area measurement, the unfamiliar reader is referred first to technical literature available from the major manufacturers of these instruments, e.g., Micromeritics Corp. and Quantachrome Corp.

nal order from $i = m$ down. Formulae exist for converting each P to the minimum equivalent channel radius ρ which a mercury meniscus can penetrate (16). By cutting the intrusion process up into contiguous narrow intervals, each of a starting and ending pressure and a starting and ending intrusion volume, one obtains a $\rho - \Delta V$ histogram wherein ρ is bounded by the limiting indicated radii and ΔV is the difference between limiting intrusion volumes of each interval. Each ΔV is transformed to specific volume by use of the specimen weight.

At the beginning of intrusion relatively few largest channels are penetrated, and it is doubtful that all existing pore networks of the largest indicated radius intervals are reached. Soon, however, a filled large-channel network is established throughout the specimen, providing an extensive and growing liquid source for reaching all remaining channels as P is further increased. Once this initial "lag" (16) is passed, the recorded ΔV values (in cm^3/g) then closely approximate the ΔV_i of pore groups as defined previously. This initial "lag" is minimized in practice by crushing the specimen into fragments, increasing the external surface area of access.

Considering the range of channel cross section shapes which may be presented to the intruding mercury, it is some challenge to relate the ρ values indicated by the porosimeter to channel cross section area. Arbitrary adjustment of the contact angle for use in the $P \rightarrow \rho$ conversion formulae has been fairly successful to this end, on average (16). A best reasonable choice for each material is here assumed.

But the bounding indicated ρ values of each interval are not necessarily bounding values of ρ_i. Each ρ interval indicated by the porosimeter is clearly an interval of effective "throat" radii in the pore network. The term "throat" has been used previously at least by Lane et al. (20) and is here preferred over the earlier term "neck" (6, 8, 9), too often associated with some idealized pore shape model. Simply as channel

constrictions halting passage of a mercury meniscus at a given pressure, "throat" and "neck" are basically synonymous. Call the ith interval of porosimeter-indicated radii an interval of ρ_{ti}, and let ρ_{ti} itself represent the mean throat radius of this ith interval.

Previously filled channels should represent the entirety of interconnected cavities larger than the upper radius of the ith interval. But these also had to be accessed via throats all larger than that upper radius as well. Channels filled in the ith interval represent the entirety of interconnected cavities accessed by throats not larger than this upper radius, but might well include larger cavities. The lower size limit, as to both cavities and their throats of access, is bounded by the lower radius of the ith interval. It is apparent that some cavities lying in the interval, or even larger, will not be filled if they are accessible only via throats falling below this lower radius limit. The measured ΔV_i thus corresponds to a measured ρ_{ti} and its interval, not to ρ_i and its interval; and ρ_i must always be at least as large as ρ_{ti}.

This depiction is mindful of the "ink-bottle" pore model of McBain (22), subject however to the reality that channel constrictions or throats can occur anywhere, either at or between pore junctions. Mercury intrusion is unable to make that distinction; nor is it mathematically important. The germane question is how to obtain a meaningful ρ_i paired with each ΔV_i, when the porosimeter gives ρ_{ti}.

A method is available to do this. But to use it requires first addressing group pore volumes at radii below ρ_μ, the throat radius corresponding to the upper pressure limit of the porosimeter. Modern 60,000 psig instruments will force Hg through oxidic throats only down to ρ_μ of roughly 1.5 nm or 15 Å. The practical lower pore-size limit of ordinary BET surface area measurement is probably well below a radius of 0.5 nm or 5 Å. The two measurements,

$$\sum_1^m \Delta V_i = V_s \text{ by porosimetry and } S_s \text{ by}$$

BET nitrogen adsorption, have to include the same limiting ρ_1.

Sophisticated BET work can fill this gap (16). Familiarity with a given material may suggest analytical means of estimating ΔV_1, . . . and ρ_1, . . . up to ρ_μ (12, 13). The best escape is assurance that there is *no* porosity below ρ_μ; and sometimes this assurance can be gained by calcining treatments which cause the smallest pores to coalesce up toward ρ_μ without appreciably altering the PSD above this limit (13). In any event, this instrumental dilemma must be addressed in some satisfactory manner, called here "extended" porosimetry, before the following can be used with precision.

2. Pore Shape Factor y and Its Use

For a given porous material, a complete set of m pore group data is presumed, consisting of $(\rho_{ti}, \Delta V_i)$ pairs determined by extended porosimetry; and a consistent S_s by BET measurement is presumed. Given that every $\rho_i \geq \rho_{ti}$, define some factor $y_i \geq 1$ such that $\rho_i = y_i\rho_{ti}$. By the mensuration formulae adopted previously, Eq. (3a) is obeyed by each ρ_i: $\Delta S_i = 2\Delta V_i/\rho_i$; hence this relation will continue to be obeyed when all m values of ΔS_i are summed. If y is now taken as a suitable mean of all y_i, then on average:

$$\Delta S_i = 2\Delta V_i/y\rho_{ti}; \tag{9a}$$

and the summation over all i is given precisely by

$$\sum_1^m \Delta S_i = S_s = \frac{2}{y}\sum_1^m \Delta V_i/\rho_{ti} = \frac{2}{y} V_s \cdot \overline{(1/\rho)}_t, \tag{9b}$$

where $\overline{(1/\rho)}_t$ is defined using only raw porosimeter data as

$$\overline{(1/\rho)}_t \equiv \sum_1^m \Delta V_i/\rho_{ti} \Big/ \sum_1^m \Delta V_i = \sum_1^m \Delta V_i/\rho_{ti} \Big/ V_s. \tag{9c}$$

With $\overline{(1/\rho)}_t$ determined by the measured data and Eq. (9c), and then inserted into Eq. (9b) with the measured V_s and S_s, y is

computed for this material. Then on average every

$$\rho_i = y\rho_{ti}; \tag{10a}$$

and

$$\bar{\rho} = y/\overline{(1/\rho)}_t; \tag{10b}$$

and

$$\overset{\circ}{\rho} = y \cdot \sum_1^m \Delta V_i\rho_{ti}/V_s. \tag{10c}$$

As $\overset{\circ}{\rho}$ can be used to obtain $D(\overset{\circ}{\rho})$ but only when porosity is unimodal (Section III), it is well to include here also the relation of $\overset{\circ}{D}$ for any PSD to the data obtained from porosimetry:

$$\overset{\circ}{D} = \sum_1^m \Delta V_i D(y\rho_{ti})/V_s. \tag{10d}$$

All of the above transformations have the common effect of moving the entire porosimeter-indicated PSD up in ρ by the constant multiplier y. Though this averaged factor may create errors in ρ_i at the tails of a PSD, at least it runs counter to the "lags" introduced there by the porosimeter (16). It creates no errors in $\bar{\rho}$ or $\overset{\circ}{\rho}$, nor likely significant errors in $\overset{\circ}{D}$. By forcing $S_s = 2V_s/\bar{\rho}$ to be obeyed for all real data, it ensures a mathematical framework consistent with the mensuration formulae and other relations of Sections II and III. In fact, the determination of $\bar{\rho}$ by Eq. (10b) with y obtained from experimental data quite satisfactorily adapts to the wide range of historical S_s/V_s ratios collected by Davis (16), as he predicted in principle that it would. Discrepancies with Eq. (3a) are thereby removed.

3. Disclosure of Noncylindrical Diffusion Paths

Computations from instrumental data by Eqs. (9c) and (9b) resulting in $y \cong 1$ clearly indicate cylindrical diffusion paths on average: not only is $\rho_i \cong \rho_{ti}$ numerically, but the physical implication is that cavities and their throats of Hg access are of about the

same size. Pore chains comprising diffusion paths are thus of relatively constant radius throughout, granting *Axiom 2* of Subsection II.3.

If y is found greater than 1, on the other hand, not only is each $\rho_i \gtrsim \rho_{ti}$ but pores or cavities of mean radius ρ_i are accessible to mercury (hence to diffusants) on average only through openings of smaller mean radius ρ_{ti}. Thus no matter how these are connected in diffusion paths, diffusants will experience changes in path cross section area reflected by the ratio ρ_i^2/ρ_{ti}^2 or y^2. Quite evidently, cylindrical paths are simply the limiting edge of a continuum of possible path types. Since by its definition y cannot be less than 1.0, an experimental finding of $y <$ 1 probably indicates error(s) in one or more of the physical measurements, including possible sampling variations. Once these causes are removed, adjustment of the Hg contact angle should be able to manage any remaining discrepancy (*16*).

The significance of noncylindrical diffusion paths to the construction of τ is that, when these occur, Eq. (4) fails and the entire series of Eqs. (4)–(8) require modification. A simplified model making these modifications possible will next be set up, utilizing these same disclosures of porosimetry.

4. A Duplex Model for Noncylindrical Diffusion Paths

A duplex model for noncylindrical porosity was originally proposed by Michaels (*23*) but without a foundation in measurable quantities. The following model is founded on the experimentally determined pore shape factor y.

When $y \cong 1$, all throats of each radius ρ_{ti} have been identified by the porosimeter with cavities of about the same radius. When $y > 1$, on average $\rho_i > \rho_{ti}$ but there is no reason to assume that *all* throats are avenues solely to larger voids. A useful postulate is, instead, that the total porosity is comprised of void populations of two different mean radii, $\bar{\rho}_t$ (measured) and $\bar{\rho}_v$

(constructed), whose overall mean is $\bar{\rho}$. The radii $\bar{\rho}$ and $\bar{\rho}_t$ are related and defined by Eq. (10b), viz., $\bar{\rho} = y\bar{\rho}_t \equiv y/\overline{(1/\rho)}_t$. For convenience analogous to this, define one more factor z by

$$\bar{\rho}_v = z\bar{\rho}_t \equiv z/\overline{(1/\rho)}_t. \qquad (11)$$

The mathematical description of this duplex model entails finding the particular combination of "pore" subsets $\bar{\rho}_t$ and $\bar{\rho}_v$ which simultaneously: (a) equates the sum of their volumes to that of the overall mean; (b) equates the sum of their surface areas to that of the overall mean; and (c) divides the total of all their inferred pore lengths, Σl, into two fractions, $\lambda\Sigma l$ (identified with subset $\bar{\rho}_v$) and $(1 - \lambda)\Sigma l$ (identified with subset $\bar{\rho}_t$). The numbers of "pores" per centimeter of body are $n_t + n_v = n_d$. Let l_d be a mean mathematical pore-length construct such that $n_v = \pi/2\lambda l_d$ and $n_t = \pi/2(1 - \lambda)l_d$.

Equations expressing conditions (a), (b), and (c) above were set up and appropriately combined. The (intrinsic) solution was found numerically for selected values of the independent parameter y; it consists of sets of simultaneous values of $l_d/\bar{l}$, of λ (hence also $1 - \lambda$), and of z. A graphical display of $l_d/\bar{l}$ vs y showed this parameter to be almost perfectly linear with y, very closely expressed by

$$l_d/\bar{l} = 4.000 - 0.320(y - 1)$$
$$= 4.320 - 0.320\,y. \qquad (12)$$

Figure 2 is a plot of the simultaneous solutions for z and for λ vs y, over a range of the latter much greater than we have found by porosimetry on various high-porosity aluminas (*12, 13*) and comparable to the range inferred from the extensive data compilation of Davis for various materials (*16*). Given an experimental $y > 1$, all quantities describing this duplex "pore" set are fixed by Eq. (12) and Fig. 2. As $y \rightarrow 1$, it is seen that the duplex set evolves into the overall mean system: $\bar{\rho}_v = \bar{\rho}_t = \bar{\rho}$ and $n_v = n_t = \bar{n}/2$.

The properties of this duplex set will be employed in Section V to obtain, finally, a

tortuosity factor τ for pore systems exhibiting noncylindrical as well as cylindrical diffusion paths.

V. CONSTRUCTION OF τ INCORPORATING NONCYLINDRICAL PATHS

It was shown in Section III that a τ computed from the overall mean properties of a pore system, namely, $\bar{n}$, $\bar{\rho}$, and $\bar{l}$, is the same as one built up from its m groups acting independently. The "overall" approach will be followed here, recognizing at the same time that the correct reference diffusivity for mass transport will be $\overset{\circ}{D}$ as given by Eq. (10d).

Consider steady-state uniaxial diffusion through a specimen Z cm in the diffusion direction by 1 cm^2, as previously. For cylindrical diffusion paths, Eqs. (4)–(8) apply. But if $y > 1$, the radius of each diffusion path is not constant. The duplex model gives, for each single diffusion path of length $\pi Z/2$, a component $\pi\lambda Z/2$ of mean radius $\bar{\rho}_v$ and a component $\pi(1 - \lambda)Z/2$ of mean radius $\bar{\rho}_t$. The diffusant transport rate, N_{Π}, must be recomputed. Call its value in the duplex path M_{Π}.

Fick's 1st Law equations are readily set up and solved for M_{Π}. It is convenient to express this as the ratio N_{Π}/M_{Π}, which is found to be

$$\frac{N_{\Pi}}{M_{\Pi}} = \lambda \cdot \frac{\bar{\rho}^2\overline{D}}{\bar{\rho}_v^2 D_v} + (1 - \lambda) \cdot \frac{\bar{\rho}^2\overline{D}}{\bar{\rho}_t^2 D_t}, \quad (13)$$

in which the D's relate to the three postulated pore sets but will be dealt with later. Replacing the squared radius ratios by their equivalents in y and z notation from Eqs. (10b) and (11), one obtains

$$\frac{N_{\Pi}}{M_{\Pi}} = y^2 \left[\frac{\lambda\overline{D}}{z^2 D_v} + (1 - \lambda) \frac{\overline{D}}{D_t} \right]. \quad (14)$$

If now M_A is defined as the duplex (noncylindrical) value of the diffusant mass transport rate per unit face area of specimen, then evidently:

$$\frac{N_A}{M_A} = \frac{\bar{n}^2 N_{\Pi}}{n_d^2 M_{\Pi}} = \frac{\bar{n}^2}{(n_v + n_t)^2} \cdot \frac{N_{\Pi}}{M_{\Pi}}. \quad (15)$$
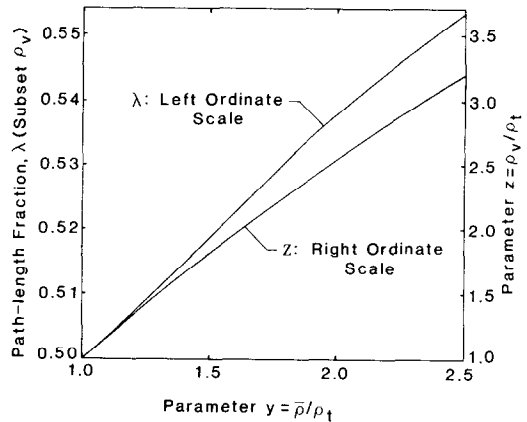

FIG. 2. Duplex pore parameters z and λ vs y.

Invoking $n_v = \pi/2\lambda l_d$, $n_t = \pi/2(1 - \lambda)l_d$, and Eq. (12) for $l_d/\bar{l}$, the above two equations are combined and transformed into

$$\frac{N_A}{M_A} = y^2(4.32 - 0.32y)^2 \left[\frac{\lambda\overline{D}}{z^2 D_v} + (1 - \lambda) \frac{\overline{D}}{D_t} \right] \bigg/ \left[\frac{1}{\lambda} + \frac{1}{1 - \lambda} \right]^2. \quad (16)$$

It is of major interest to examine N_A/M_A at this point. Using Fig. 2 for z and λ, Eq. (16) is most conveniently solved numerically. However, in doing so, it is necessary to consider some characteristic values of the diffusivity ratios in it.

Those ratios are unity if all diffusivities are D_b. This limiting case occurs for a gaseous diffusant when (in unimodal porosity) the mean pore radius $\overset{\circ}{\rho}$ is above about 5 times the gas mean free path (12); or for liquid diffusants above the onset of "hindered diffusion" (3–5), i.e., above about 25 times the liquid diffusant molecular radius.

When ideal Knudsen diffusion is in effect for gases (6, 7), these ratios can be readily shown to be $\overline{D}/D_v = \bar{\rho}/\bar{\rho}_v = y/z$ and $\overline{D}/D_t = \bar{\rho}/\bar{\rho}_t = y$. This situation occurs when $\overset{\circ}{\rho}$ is below about 0.05 times the gas mean free path (12).

Figures 3 and 4 are plots of N_A/M_A computed from Eq. (16) for these two cases. When bulk diffusion governs (Fig. 3), the plot of N_A/M_A vs y is curvilinear near the
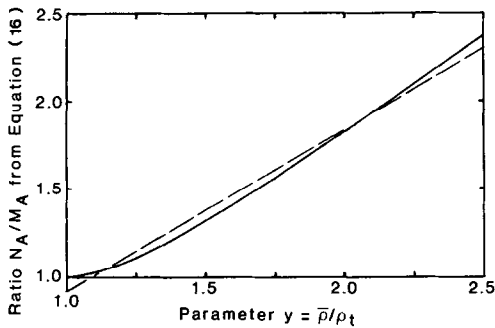
FIG. 3. N_A/M_A vs y: bulk diffusion governing.

(1, 1) origin but near-linear for all $y > 1.5$. In spite of the curvature, however, the linear approximation given by the dashed curve, which is $N_A/M_A = 0.92y$, is good to better than $\pm 5\%$ everywhere except near $y = 1.0$ where a noncylindrical model is unnecessary in any event. One accordingly inserts Eq. (6) for N_A into this relation and rearranges explicit in M_A, obtaining:

$$M_A = \frac{-f}{0.92y \cdot 2.47(1 - 4\bar{\rho}/3\bar{l}\,)} \cdot \overset{\circ}{D} \cdot \Delta c/Z.$$
(17)

From the identity of Eqs. (7) and (8) it follows that, with x given by Eq. (8):

$$\tau = 0.92xy.$$
(18)

When ideal Knudsen diffusion governs (Fig. 4), the plot of N_A/M_A vs y^2 is comparably near-linear. The dashed curve used as approximation in this figure is $N_A/M_A = 0.846y^2 = 0.92^2y^2$. Again the only significant error occurs near $y = 1.0$, whereas again a noncylindrical model is inappropriate there. By insertion of Eq. (6) into this simple function and rearranging, one obtains

$$M_A = \frac{-f}{0.92^2y^2 \cdot 2.47(1 - 4\bar{\rho}/3\bar{l}\,)} \cdot \overset{\circ}{D} \cdot \Delta c/Z.$$
(19)

Again using Eqs. (7) and (8) interchangeably, it follows that:

$$\tau = x(0.92y)^2.$$
(20)

Finally, by mathematical inference from Eqs. (18) and (20) and incorporating Eq. (8) for x, one can write a general equation for τ as

$$\tau = x \cdot (0.92y)^{1+\varepsilon} = (2.23 - 1.13V_s d)$$
$$\cdot (0.92y)^{1+\varepsilon},   (21)$$

where ε is the slope of a log–log plot of $D(\rho)$ vs ρ at $D = \overset{\circ}{D}$.

In the simplicity of its form, resulting from some very acceptable approximations, Eq. (21) leaves the tedium of its development entirely behind. Its few parameters are readily obtainable by measurement. One just drops the last bracket, $(0.92y)^{1+\varepsilon}$, when $y < 1.1$. With that adjustment Eq. (21) serves equally for cylindrical and noncylindrical diffusion paths as disclosed by y, and for any PSD. As discussed in Section III, $\overset{\circ}{D}$ may be replaced by $D(\overset{\circ}{\rho})$ in diffusion equations only if the PSD in unimodal. The next Section describes practical usages of Eq. (21).

VI. PRACTICAL COMPUTATIONS OF τ

For any ordinary material capable of porosity characterization by mercury porosimetry, the data needed for computation of its tortuosity factor consist of:

(a) Its extended porosimetry $\rho_{ti} - \Delta V_i$ data over all i, and $\sum\limits_{1}^{m} \Delta V_i = V_s$;
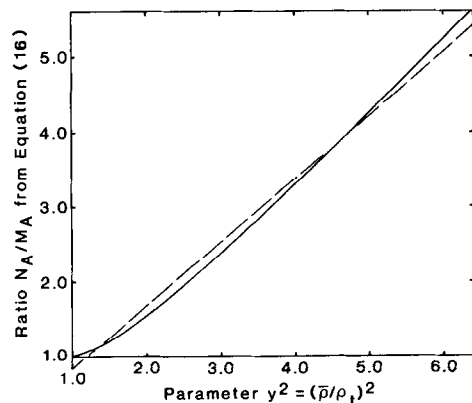

FIG. 4. N_A/M_A vs y^2: Knudsen diffusion governing.

(b) Its total BET specific surface area, S_s;

(c) Its nominal density, d; and

(d) A log–log plot of $D(\rho)$ vs ρ for the diffusant system and conditions of interest.

One then carries out the following operations in sequence:

(A) Enter V_s and d into Eq. (8) to obtain the quantity "x;"

(B) From the raw porosimeter data, determine $\overline{(1/\rho)}_t$ by Eq. (9c);

(C) Enter $\overline{(1/\rho)}_t$, V_s, and S_s into Eq. (9b) to obtain the quantity "y;"

(D) If $y < 1.1$, then $\tau = x$. Execute (E) to obtain $\overset{\circ}{D}$, then stop.

(E) If $y > 1.1$, from the $D(\rho)$ vs ρ curve determine $D(y\rho_{ti})$ for every ρ_{ti} of the porosimetry data and perform the arithmetic of Eq. (10d) to obtain $\overset{\circ}{D}$;

(F) Enter $\overset{\circ}{D}$ on the log–log plot of $D(\rho)$ vs ρ and obtain the slope there, which is "ε;"

(G) Enter x, y, and ε into Eq. (21) to determine τ.

If $\overset{\circ}{\rho}$ is sought instead (for unimodal porosity), then (E) is simpler: using the porosimetry data with y, obtain $\overset{\circ}{\rho}$ by Eq. (10c). The $D(\overset{\circ}{\rho})$ and the log–log slope at $D(\overset{\circ}{\rho})$ are obtained from the diffusivity curve, and (G) follows.

Experience (13) indicates that the porosimeter intervals should not exceed a radius ratio (max. to min. of the interval) of $1.5:1$. If this is observed, ρ_{ti} can safely be taken as the logarithmic mean of the interval: it will be within 2% of either the ordinary or the inverse mean. A total number of intervals (i.e., m) of 20 to 25 should ordinarily be sufficient; these need not be of (logarithmically) equal width. The numerical operations entailed in obtaining τ as above are tedious if performed manually, but can readily be reduced to machine calculation in most cases. In porosimetry on aluminas, we have used Hg contact angles of 135° to 140°.

Many porous materials of interest in catalysis are bimodal, the micropores (i.e., mode "1") and macropores (mode "2")

arising relatively independently from different aspects of their processing history. Some approaches to diffusion kinetics have preferred to treat the two pore sets quite separately (e.g., (10)). To do this requires separate f_1 and f_2, $D(\overset{\circ}{\rho}_1)$ and $D(\overset{\circ}{\rho}_2)$, and τ_1 and τ_2. But the procedure developed here for computing τ is based on a y obtained from the entire PSD. If separate τ_1 and τ_2 are to be computed, in consistent notation separate x_1 and x_2, y_1 and y_2, and ε_1 and ε_2 are needed. Since intraparticle micropores and interparticle macropores are parallel but independent sets (10), Eq. (8) suffices (with f_1 and f_2) to produce x_1 and x_2; and ε_1 and ε_2 present no problem. But without very sophisticated BET work there is no effective way to obtain y_1 and y_2 from measured properties of the porosity. Such BET work entails additional problems (16).

A way has been found to circumvent this dilemma. Usually the micropore mode is relatively narrow in such materials (11, 24). When this is so, y_1 can be estimated between 1.0 and 1.2. Given the isolated modal V_{s_1} from porosimetry and the estimated y_1, Eq. (9b) can be solved for the modal S_{s_1}. This is then subtracted from the measured total S_s, the difference S_{s_2} attributed to the macropores. Then all data are in hand permitting the determination of y_2. Separate computations of τ_1 and τ_2 by Eq. (21) are thereby facilitated: note that in this case, $\tau_1 \cong x_1$.

An example of this device is included in Subsection VII.2, giving reassuring results. In most cases of kinetic analysis (e.g., (11, 12)) the PSD is not treated as isolated modes, and this device is unnecessary. The physical data of (a)–(d) above and the numerical operations of (A)–(G) above are sufficient, giving an overall τ.

VII. TESTS OF THE COMPUTED τ

1. Comparison With Diffusion-Determined Values at Large

We do not presently determine τ by diffusion, so direct comparison in materials for

TABLE 1

Present Computed τ vs Diffusion-Determined Values: Various Oxidic Materials and Catalysts

Materials[a]	Original data[b]		Present computations by Eq. (21)[b]			
	f	τ	τ	x	y	ε
Unbonded compacts (300)	0.31	1.8	1.9	1.88	1.0	—
Unbonded compacts (300)	0.22	2.5	2.45	1.98	1.3	0.2
Leached Vycor (19,118,199,166,260)	0.30±	5.9	5.8±	1.89±	1.9±	1.0
Leached Vycor (141,310,360)	0.29±	3.1–10.5	5.8±	1.90±	1.9±	1.0
γ-Alumina (293)	0.38–0.53	3.7±	3.2±	1.7±	1.5±	1.0
Refractory oxide (293)	0.115	2.9	3.4±	2.10	1.5±	0.5
Silicas and silica–aluminas (122,308,348)	0.47±	2.1– 5.7	3.3±	1.70±	1.5±	1.0
Silicas and silica–aluminas (122,377)	0.50±	2.3– 4.6	3.2±	1.66±	1.5±	1.0
Silicas and silica–aluminas (122)	0.56±	2.5– 3.4	3.0±	1.59±	1.5±	1.0
Silicas and silica–aluminas (122)	0.68	2.1	2.4±	1.46	1.4±	1.0
Silica–alumina catalysts (378)	0.35±	7.4– 8.7	5.6±	1.84±	1.9±	1.0
Silica–alumina catalysts (378)	0.5±	1.6– 4.7	3.0±	1.6±	1.5±	1.0
Silica–alumina catalysts (39)	0.52	2.7– 3.8	3.1±	1.64±	1.5±	1.0
Chromia–alumina catalysts (293)	0.45	4.4	3.3±	1.72	1.5±	1.0
Chromia–alumina catalysts (378)	0.56±	1.6±	1.6±	1.6±	1.0	—
Supported metal catalysts (293)	0.41±	2.8– 3.9	2.9–3.3	1.76±	1.5±	0.5–1.0
Supported metal catalysts (293)	0.49±	7.2±	5.1±	1.67±	1.9±	1.0
Hydroprocessing catalysts (293)	0.35	4.8±	5.0±	1.83	1.9±	0.8
Hydroprocessing catalysts (293)	0.39	3.9	4.1±	1.79	1.9±	0.5
Hydroprocessing catalysts (293)	0.41	3.8	5.4±	1.77	1.9±	1.0
Hydroprocessing catalysts (293)	0.49	7.1	5.1±	1.68	1.9±	1.0

[a] Reference numbers given in (6).

[b] "±" = typ. 1–3 in last significant figure.

which we have determined y is not possible. However, we have enough experience in porosimetry (13) to permit the estimation of y, given even rudimentary information describing porous oxides. Satterfield (6) has collected gas-diffusion-measured τ values for a host of these, together with sufficient other data for the independent estimation of τ by Eq. (21). A comparison of the computed values and their makeup with the original τ values (6) is shown in Table 1. Here, x is obtained from the given f; y is estimated from the descriptive information (6), lacking porosimeter histograms; and ε is estimated from indications (6) of the diffusion region (bulk, Knudsen, or mixed) governing in each case. Agreement between the present computed τ values and the original diffusion-determined values is on the whole remarkable.

2. Application to Diffusion Data of Wakao and Smith

These authors (10) made five essentially unbonded pseudoboehmite alumina compacts, "A, ———, E," by techniques which in general affected only the macroporosity of a bimodal distribution. They measured binary (N_2, He) gas diffusion through these at successively higher total pressures, "1, 2, 3, ———." Their premise in treating diffusion kinetics was, in present notation, $D_{\text{eff}} = f^2 D(\mathring{\rho})$ separately for each pore mode. From this premise it has been inferred (e.g., (6)) that $\tau = 1/f$. Besides the difficulty with this mentioned in Section I, taken literally with their f_2 data it results in τ_2 values running up to >11. The present methods imply improved interpretation of porosimetry relative to their "shifted block" model as well

TABLE 2

Nitrogen Diffusion Data of Wakao and Smith Treated by Present Method

		Micropores			Macropores					Σ $M_A \times 10^4$	Obs. [10] $M_A \times 10^4$
	f_1 (cm^3/cm^3)	$\rho_t = \bar{\rho} = \rho_v$, (A) [24]	$M_{A_1} \times 10^8$ (mole/cm^2 sec)	f_2 (cm^3/cm^3	$y_2 = \rho/\rho_t$	x_2	τ_2	$M_{A_2} \times 10^4$ (mole/cm^2 sec)			
A 1	0.17	20.	1.00	0.63	1.20	1.51	1.67	0.0243		0.0244	0.0247
2			1.72					0.0235		0.0237	0.0235
3			3.77					0.0300		0.0304	0.0320
4			5.38					0.0306		0.0311	0.0334
B 1	0.27	20.	2.03	0.45	1.42	1.71	2.40	0.00973		0.00993	0.00957
2			7.75					0.01237		0.01315	0.01293
C 1	0.33	20.	5.52	0.34	1.46	1.83	2.88	0.00763		0.00818	0.00805
2			10.70					0.00868		0.00975	0.00983
D 1	0.39	20.	4.32	0.18	1.55	2.03	3.83	0.00157		0.00200	0.002112
2			10.79					0.00275		0.00383	0.003631
3			11.75					0.00276		0.00394	0.003947
4			17.48					0.00315		0.00490	0.004914
E 1	0.42	20.	7.51	0.09	1.83	2.15	6.07	0.00060		0.00135	0.001409
2			15.66					0.00093		0.00250	0.002408

as adaptation to its implicitly noncylindrical porosity, neither being available at the time of their work. Accordingly, it was felt useful to try the present construction of τ on their specimens.

The published data (10), even augmented by a companion paper by Mischke and Smith (24), were of insufficient detail for the determination of y by Eq. (9b). However, y_1 for micropores can be taken as about 1 by the device mentioned in Section VI, and y_2 could be estimated for each of Compacts A to E from our experience (13). From the given f_1 and f_2 (10), x_1 and x_2 were determined by Eq. (8) and τ_1 was accordingly taken as $\tau_1 = x_1$. For τ_2, ε_2 was estimated for each compact by the original methods (10) but using a y-corrected $\bar{\rho}$ value for $D(\bar{\rho})$ in place of each original $\bar{\rho}$. Then with each x_2, y_2, and ε_2 in hand, τ_2 was computed by Eq. (21).

Contrary to the view originally taken (10), it is felt that the all-micropore and the micro-macropore diffusion paths are one and the same in these compacts. This reduced the number of transport computations to two (viz., all-micro and all-macro),

with no significant quantitative effect in four of the five materials since macropore transport was dominant in these. The binary N_2 diffusion equations (10) were used to compute the areal micropore and macropore mass transport rates for each material and conditions of diffusion, and these were summed to give the total areal N_2 mass transport for comparison with each measured value (10).

Table 2 lists the most important present computation results, accompanied by a minimum of the original data. The results are gratifyingly consistent, both internally and by comparison with the experimentally observed N_2 transport data (cf. last two columns). Original data taken (10) at pressures much in excess of 5 atm were not used in this exercise, since those tabulated seem sufficient.

Table 2 indicates τ_2 values all within the ordinary range for aluminas, as computed by the present methods (13) or compared with Table 1. Wakao and Smith graphically illustrated a linear empirical semilog relation between their $\bar{\rho}_2$ and pore volume fraction f (10), that could have confounded ρ-

dependencies of transport properties with f-dependencies and hence made their premise $D_{eff} = f^2 D(\overset{\circ}{\rho})$ appear reasonable. But other material fabrication methods (especially, of bonded materials) generally do not produce the same correspondence; hence their premise and its suggestion that $\tau = 1/f$ is probably contraindicated unless proved applicable. Table 2 shows that even then it is unnecessary. The classical relation $D_{eff} = (f/\tau)D(\overset{\circ}{\rho})$ appears quite upheld here without using an imputed relation between τ and f alone.

A similar analysis of the recent N_2 gas permeation data of Valuš and Schneider, (11) who used compacts also formed of pseudoboehmite but calcined to $\alpha\text{-Al}_2\text{O}_3$, was reinforcing to the above suggestions. These authors expressed difficulty in determining τ by their model; but the present analysis indicated that (a) τ increased regularly from 2.75 to 3.49 with increasing forming pressure at fixed calcining $T = 1200°C$, and (b) τ behaved somewhat irregularly but started at 2.79 and ended at 2.68 for a series of lightly compacted specimens calcined at temperatures increasing regularly from 1200°C up. Again, all these τ values are perfectly reasonable for aluminas, and are in accord with the measured N_2 transport data (11). In neither of these series of specimens is $\tau = 1/f$ (or $\tau_2 = 1/f_2$ by inference) even close.

VIII. CONCLUSIONS

The present mathematical development has resulted in a simple equation for the numerical computation of τ, calling for ordinary physical property data for porous materials and ordinary diffusant systems. This equation is easy and economical to use and realistic in its physical construction. It relates τ understandably to its contributing properties including the measurable occurrence of "noncylindrical" porosity. It does demand a departure from past relatively lax approaches to instrumental porosimetry, engendered by past inability to make informed use of it.

Computed τ values using this equation are in good agreement with those measured by diffusion for a large number of catalysts and other porous materials described in the literature. This work has emphasized the fundamental relationship $D_{eff} = \overset{\circ}{D} \cdot f/\tau$, with $\overset{\circ}{D}$ explicitly defined; and has shown that $\overset{\circ}{D}$ may be replaced by $D(\overset{\circ}{\rho})$ only in limited circumstances, with $\overset{\circ}{\rho}$ also carefully defined in relation to the direct output of Hg porosimetry. Application has been shown equally successfully to the entire porosity of a material and, severally, to the isolated modes of bimodal porosity.

Surface diffusion as limiting is not encompassed, and available tests do not include extremely high-pressure diffusant systems. Computation of τ by the given equation is accordingly recommended at this time for "moderate" diffusion conditions.

APPENDIX NOMENCLATURE

D diffusivity. D_b: bulk value. $D(\rho)$: function of path radius ρ. $D(\overset{\circ}{\rho})$: value of $D(\rho)$ at $\rho = {}_o\overset{\circ}{\rho}$. $D(\rho_i)$: value of $D(\rho)$ at $\rho = \rho_i$. $\overset{\circ}{D}$: mean of $D(\rho_i)$ over all ρ_i

M mass transport rate in duplex (noncylindrical) diffusion paths. M_A: areal value through all porosity. M_{Π}: value in any one duplex path

N mass transport rate in cylindrical diffusion paths. N_A: areal value through all porosity. N_{Ai}: areal value through all paths of radius ρ_i. N_{Π}: average value in a single path. $N_{\Pi i}$: value in one path of radius ρ_i

PSD   pore size distribution: a set of paired $(\rho_i, \Delta V_i)$ or $(\rho_{ti}, \Delta V_i)$ data for every i from 1 to m in a given material, obtained by Hg-porosimetry extended to $i = 1$

S_s specific surface area of all porosity in a body

ΔS_i specific surface area of all porosity of the ith size group (radius ρ_i) in a body

V_s specific void volume of all porosity in a body

ΔV_i specific void volume of all porosity of the ith size group (radius ρ_i) in a body

Z length of a body or specimen in the direction of uniaxial diffusion through it

c concentration of a diffusant at a given point or station

d nominal density of a porous body: weight/nominal (external) volume

f void volume fraction of all porosity in a body

Δf_i void volume fraction of all porosity of the ith size group (radius ρ_i) in a body

i integer designating one of a set of contiguous pore size groups or pore radius intervals from smallest ($i = 1$) to largest ($i = m$) present in a given body

l pore length between adjacent junctions. $\bar{l}$: average of all l_p. l_d: a construct used in a postulated duplex (noncylindrical) model. l_i: average of l_p for all pores of the ith size group. l_p: length of any one pore

m number of pore size groups comprising a total porosity; or, the index i of the largest group present in a body

n number of pores per centimeter of body, defined by n^3, the number of pores in 1 cm^3 of body. $\bar{n}$: total representing all porosity. n_d: total of postulated duplex (noncylindrical) pore set. n_i: total of all pores of the ith size group. n_t and n_v: totals of the smaller and larger subsets, respectively, of a duplex set

s pore-wall surface area. $\bar{s}$: average of all s_p. $\bar{s}_i$: average of s_p of all pores of the ith size group. s_p: surface area of any one pore

v pore volume. $\bar{v}$: average of all v_p. $\bar{v}_i$: average of v_p of all pores of the ith size group. v_p: volume of any one pore

x a factor of τ as constructed; a specified function of $f = V_s d$

y a factor of τ as constructed; determined from extended porosimetry and surface area data

z the ratio $\bar{\rho}_v / \bar{\rho}_t$ in a postulated duplex (noncylindrical) pore set; function of y

α acute angle made between l_p of any pore and the macroscopic diffusion axis

ε exponent of y appearing in τ as constructed; obtained from $D(\rho)$ vs ρ data

λ fraction of Σl or of l_d comprised of all larger pores (see $\bar{\rho}_v$) of a postulated duplex, noncylindrical set. $(1 - \lambda)$: fraction comprised of all smaller pores ($\bar{\rho}_t$) of that set

ρ radius or effective radius of a pore or cavity or a connected chain or channel of same. $\mathring{\rho}$: volume-weighted mean of all ρ_p hence of all ρ_i. $\bar{\rho}$: volume-weighted inverse mean of all ρ_p or all ρ_i. $\bar{\rho}_t$: mean of all smaller pores of a postulated duplex, noncylindrical pore set. $\bar{\rho}_v$: mean of all larger pores of the duplex pore set. ρ_i: mean of a narrow radius interval defining the ith pore size group. ρ_1: mean of the smallest pore size group present, $i = 1$. ρ_m: mean of the largest pore size group present, $i = m$. ρ_μ: smallest radius penetrable by a mercury porosimeter. ρ_p: radius of any one pore. ρ_{ti}: mean of a narrow radius interval as indicated by the Hg porosimeter, hence of "throats" in the pore network, defining the ith pore size group

τ tortuosity factor, defined by $D_{eff} = \mathring{D} \cdot f/\tau$; as constructed here, for the total porosity of a body or specimen. τ_c: value of τ for the special case of cylindrical diffusion paths. τ_1: τ computed separately for the micropore mode of a bimodal PSD. τ_2: τ computed separately

for the macropore mode of a bi-modal PSD

REFERENCES

1. Scott, D. S., and Dullien, F. A. L., *AIChE J.* **8,** 113 (1962).
2. Evans, R. B., Watson, G. M., and Mason, E. A., *J. Chem. Phys.* **35,** 2076 (1961).
3. Chantong, A., and Massoth, F. E., *AIChE J.* **29,** 725 (1983).
4. Satterfield, C. H., Colton, C. K., and Pitcher, W. H., *AIChE J.* **19,** 628 (1973).
5. Beck, R. E., and Schultz, J. S., *Science* **170,** 1302 (1970).
6. Satterfield, C. H., "Mass Transfer in Heterogeneous Catalysis." M.I.T. Press, Cambridge, Mass., 1970.
7. Wheeler, A., *in* "Advances in Catalysis" (W. G. Frankenburg, V. I. Komarewsky, and E. K. Rideal, Eds.), Vol. 3, 249. Academic Press, New York, 1951.
8. Currie, J. A., *J. Appl. Phys. Brit.* **11,** 318 (1960).
9. Petersen, E. E., *AIChE J.* **4,** 343 (1958).
10. Wakao, N., and Smith, J. M., *Chem. Eng. Sci.* **17,** 825 (1962).
11. Valuš, J., and Schneider, P., *Appl. Catal.* **16,** 329 (1985).
12. Carniglia, S. C., *Appl. Catal.* **14,** 343 (1985).
13. Carniglia, S. C., Pearson, M. J., and Rigge, R. J., Kaiser Aluminum & Chemical Corp., Pleasanton, Calif., unpublished work.
14. Johnson, M. F. L., and Stewart, W. E., *J. Catal.* **4,** 248 (1965).
15. Satterfield, C. H., and Cadle, P. J., *Ind. Eng. Chem. Fundam.* **7,** 202 (1968).
16. Davis, B. H., *Appl. Catal.* **10,** 185 (1984).
17. Grachev, G. A., Ione, G. K., and Barshev, A. A., *Kinet. Katal.* **11,** 1041 (1970).
18. Corrie, J., Orhon, M., and Trimm, D. L., *J. Chem. Eng. Lausanne* **6,** 74 (1973).
19. Cormack, D. E., and Beattie, C. I., *Chem. Eng. Sci.* **34,** 1001 (1979).
20. Lane, A., Shah, N., and Conner, W. C., *J. Colloid Interface Sci.* **109,** 235 (1986).
21. Sahimi, M., and Tsotsis, T. T., *J. Catal.* **96,** 552 (1985).
22. McBain, J. W., *J. Amer. Chem. Soc.* **57,** 699 (1935).
23. Michaels, A. S., *AIChE J.* **5,** 270 (1959).
24. Mischke, R. A., and Smith, J. M., *Ind. Eng. Chem. Fundam.* **1,** 288 (1962).